# NASA TECHNICAL MEMORANDUM 100622

# MECHANICS OF INSTABILITY-RELATED DELAMINATION GROWTH

John D. Whitcomb

May 1988



NASA
National Aeronautics and
Space Administration

**Langley Research Center**
Hampton, Virginia 23665

## INTRODUCTION

When a laminate containing a near-surface delamination is subjected to compression loads, local buckling of the delaminated region can occur. This buckling causes load redistribution and secondary loads, which in turn cause interlaminar stresses. Delamination growth resulting from these interlaminar stresses is referred to herein as instability-related delamination growth (IRDG). Fig. 1 shows two configurations which exhibit IRDG: uniaxially loaded laminates with a through-width or embedded delamination. Typical analytical studies of these configurations can be found in refs. 1-8. The case of a circular embedded delamination with axisymmetric loads has also been examined (ref. 9). The mechanics of IRDG have been described for the through-width delamination in refs. 2 and 4. Herein, the term "mechanics of IRDG" refers to the process by which load is redistributed and secondary loads are created. A description of the mechanics of IRDG includes much more than assemblying the governing equations, solving them, and obtaining some values for the strain-energy release rates. Unless an intuitive feel for IRDG is acquired, even exact answers for idealized configurations are of limited use. Earlier studies of the embedded delamination have presented various analyses, but the mechanics of IRDG have not been addressed. The purpose of this paper is to describe the mechanics of IRDG for the embedded delamination.

Because the stresses are singular along the delamination front, point values of the stresses are of limited use. Strain-energy release rates are finite parameters which quantify the intensity of the stresses at the delamination front. In this paper it will be assumed that the magnitude of the strain-energy release rates govern delamination growth. Consequently, the mechanics of IRDG will be discussed in terms of its influence on strain-energy release rates.

The stress analysis used in this study was a geometrically nonlinear three-dimensional finite element program (NONLIN3D, ref. 8). The following sections will begin with a brief description of NONLIN3D, the finite element models, and the material properties. Then typical strain-energy release rate results will be shown for four configurations which exhibit IRDG. The four configurations are the through-width delamination, the embedded delamination with axisymmetric loads, and circular and elliptical embedded delaminations with uniaxial loads. These strain-energy release rates will be used to illustrate the distinct differences in behavior exhibited by the configurations. Then the mechanics of IRDG will be discussed. First the mechanics of IRDG for the through-width delamination will be reviewed. Then its close relationship to the axisymmetrically loaded embedded delamination is explained. A laminate with a through-width delamination can be transformed into a laminate with an embedded delamination by applying appropriate tractions. The mechanics of IRDG for the embedded delamination will be explained by considering the type and sign of traction required. The differences in the strain-energy release rates for the four configurations will be discussed in terms of the mechanics of IRDG.

## NOMENCLATURE

| | |
|---|---|
| a, b | Semi-axes of elliptical delamination in x and y directions, respectively |
| $C_{ij}$ | Constitutive coefficients |
| $E_{11}$, $E_{22}$, $E_{33}$ | Young's moduli for orthotropic material |
| $F_y$,$F_z$ | Forces in y- and z-directions, respectively |
| $G_I$, $G_{II}$ | Mode I and mode II total strain-energy release rate |
| $G_{12}$, $G_{23}$, $G_{13}$ | Shear moduli for orthotropic material |
| h | Thickness of sublaminate |
| H | Thickness of base laminate |
| $M_y$ | Moment about y axis |
| u, v, w | Displacements in x-, y-, and z-directions |
| W | Length and width of the square finite element model |
| x, y, z | Cartesian coordinates |
| $\alpha$ | Angle between local and global coordinate systems |
| $\varepsilon_o$ | specified axial strain |
| $\nu_{12}$, $\nu_{23}$, $\nu_{13}$ | Poisson's ratios for orthotropic material |

## ANALYSIS

This section will give a brief description of the finite element program used to obtain the strain-energy release rates presented herein. The finite element program, which is named NONLIN3D was developed at NASA Langley Research Center. Further details may be found in ref. 8. Also, a typical finite element model and the material properties will be described.

### The Finite Element Program NONLIN3D

NONLIN3D is a three-dimensional, geometrically nonlinear finite element program. The primary type of geometric nonlinearity considered is that due to significant rotations. This is accounted for by using the Lagrangian nonlinear strain-displacement relations (ref. 10). The governing equations were derived by minimization of the total potential energy. A Newton-Raphson iterative procedure was used to solve the nonlinear governing equations.

Figure 2 shows two typical finite element models. The same 2D mesh was used to generate both of the models shown. Hence, the close-up in fig. 2a is also valid for fig. 2b. The elements are 20-node isoparametric hexahedra. The sublaminate thickness h was one-tenth of the base laminate thickness H. Because of symmetry only one-fourth of the specimen was modeled and the constraints $u = 0$ on $x = 0$ and $v = 0$ on $y = 0$ were imposed. There was also a constraint $w = 0$ on $z = 0$. This constraint was imposed to remove global bending from the analysis. In reality, there might be global bending (particularly if the buckled region is thick), but the amount of global bending would depend on the size of the region modeled and the boundary conditions at the external boundaries. Imposing $w = 0$ on $z = 0$ simply removed overall specimen size and external boundary conditions as parameters to be considered in this study. The constraint on $w$ represents a laminate which is well constrained globally. Of course, one could also view the constraint $w = 0$ on $z = 0$ as an indication of symmetry about the $z = 0$ plane. This implies the presence of two delaminations.

Along the boundary $x = W$, all $u$ displacements are specified to equal $x\varepsilon_o$, where $\varepsilon_o$ is the specified compressive axial strain. To initiate transverse deflections, a transverse load was applied at the center of the delaminated region. After a converged solution was obtained, the load was removed, and solutions were obtained with only compression loading.

The model for the axisymmetric load case differed only in that equal displacements were prescribed along both x=W and y=W to obtain biaxial compression. This biaxial loading results in axisymmetric loading of the delaminated region.

The model for the through-width delamination is shown in fig. 2b. Since this case is basically 2-D, a 2D analysis was performed. In order to perform a two-dimensional analysis using NONLIN3D, v was prescribed to be zero on the planes y=0 and y=W. This restricted

the model behavior to 2-D plane strain. The through-width delamination case is trickier to analyze than the other cases because the tangential stiffness of the buckled sublaminate is essentially zero. This results in a singular stiffness matrix. Refs. 2 and 11 describe the procedure used to circumvent this problem.

To reduce the computational effort, substructuring was used. Most of the postbuckled region was in one substructure and the remainder of the laminate was in the other substructure. Fig. 3 shows a typical division of the laminate. The boundary between the two substructures was a distance "$\ell$" behind the delamination front. The length $\ell$ was approximately equal to the sublaminate thickness h . Since significant rotations occur only in the buckled region, a nonlinear analysis was required only in one substructure. A reduced stiffness matrix and load vector were obtained for the linear substructure and these were used to augment the equations for the nonlinear substructure.

Strain-energy release rates were the primary output from the analysis. The strain-energy release rates were calculated using a three-dimensional version of the virtual crack closure technique in ref. 13. The strain-energy release rates were calculated relative to a local coordinate system. The local coordinate system for the circular and elliptical delaminations is shown in fig. 4. One axis is normal to the delamination front and one axis is tangent. For all the cases considered, the local z-axis was parallel to the global z-axis. The angle between the local and global y-axes is $\alpha$.

**Material Properties**

The intent of this paper is to consider only the effect of geometric parameters on the mechanics of IRDG. Consequently, material properties were chosen to minimize the effect of material properties. For quasi-isotropic laminates the in-plane stiffness is independent of direction. But even for quasi-isotropic laminates the flexural stiffness varies with direction. Hence, even if the postbuckled region consisted of a quasi-isotropic group of plies, one would expect variations in the strain-energy release rate along the delamination front which are caused solely by the variation in flexural stiffness. Also, the properties of the interface plies (i.e., those plies on either side of the delamination) would be expected to at least affect the relative magnitudes of $G_I$, $G_{II}$, and $G_{III}$.

The simplified material properties chosen for this study are those for a "homogeneous quasi-isotropic laminate". These properties $\overline{C}_{ij}$ are obtained as follows:

$$\overline{C}_{ij} = \frac{1}{8}\sum_{\ell=1}^{8}(C_{ij})^{\ell}$$

where $(C_{ij})^{\ell}$ are the constitutive properties for the $\ell^{th}$ ply in the 8-ply quasi-isotropic laminate $(\pm 45/0/90)_s$. With these properties, there are no stacking sequence effects and

no variation of material properties with orientation. These properties are not isotropic, since there are still reduced transverse shear and extension moduli.

The lamina properties were selected to be typical of graphite/epoxy (ref. 12). The moduli and Poisson's ratios are:

$$E_{11} = 134 \text{ GPa}$$
$$E_{22} = E_{33} = 10.2 \text{ GPa}$$
$$G_{12} = G_{13} = 5.52 \text{ GPa}$$
$$G_{23} = 3.43 \text{ GPa}$$
$$\nu_{12} = \nu_{13} = .3$$
$$\nu_{23} = .49$$

## COMPARISON OF BEHAVIORS FOR THE THROUGH-WIDTH AND THE EMBEDDED DELAMINATION

Four cases were analyzed: the through-width delamination, the axisymmetrically loaded embedded circular delamination, the uniaxially loaded embedded circular delamination, and the uniaxially loaded embedded elliptical delamination. In all cases the thicknesses H and h were 4 and .4 mm, respectively. The through-width delamination was 30mm long. The circular delaminations were 30mm in diameter. The elliptical delamination was elongated along the y-axis and had dimensions of 30x60mm. The same strain range was used for all the cases.

Figures 5 and 6 show the effect of strain level on $G_I$ and $G_{II}$ for the through-width delamination and the embedded delamination. The mode III component is not shown because it was essentially zero for all the cases considered. In general, one would not necessarily expect $G_{III}$ to be zero. Both uniaxial and axisymmetric loads were considered for the embedded delamination. For the uniaxially loaded embedded delamination both a circular and an elliptical delamination were analyzed. Figs. 5c, 5d, 6c, and 6d show the variation with strain level at two points along the delamination front of the uniaxially loaded embedded delamination: at $\alpha = 0^o$ and $\alpha = 90^o$. See fig. 4 for the definition of alpha.

The variation of $G_I$ with strain level is dramatically different for the four cases. For the through-width delamination $G_I$ increases very rapidly after buckling occurs.(fig. 5a) After reaching a peak, $G_I$ decreases. For the axisymmetric case, $G_I$ increases monotonically. Also, the magnitude of $G_I$ in fig. 5b is much larger than in fig. 5a.

Fig. 5c shows the variation of $G_I$ at $\alpha = 90^o$ for a uniaxially loaded embedded delamination. Only the results for the elliptical delamination are shown here, since $G_I$ was zero at $\alpha = 90^o$ for all strain levels for the circular delamination. The shape of the

curve for the elliptical delamination is similar to that for the through-width delamination (fig. 5a), but the magnitude is less. At $\alpha = 0^o$, $G_I$ is shown for both the circular and elliptical delaminations (fig. 5d). Note that the magnitude of $G_I$ is much larger than in figs. 5a-5c. Also, $G_I$ increases rapidly and monotonically with applied strain.

Fig. 6 shows the $G_{II}$ variations with strain level. In all cases $G_{II}$ increased monotonically with strain. $G_{II}$ is of the same order of magnitude for all the cases except for the uniaxially loaded circular delamination at $\alpha = 90^o$ (fig. 6c). This contrasts with the very wide range of magnitudes in fig. 5 for $G_I$.

Even though the strain-energy release rates in all the cases illustrated in figs. 5 and 6 are a result of local buckling, the variety of behavior suggests that there must be variations in the mechanism by which local buckling causes strain- energy release rates. The next section will attempt to explain these mechanisms.

## MECHANICS OF IRDG FOR THE EMBEDDED DELAMINATION

In highly simplified anthropomorphic terms, a strip of the buckled region which is parallel to the load direction (strip A in fig. 7) wants to buckle outward. A strip of the buckled region which is perpendicular to the load direction (strip B in fig. 7) has no desire to deform outward; it is pushed out by strip A. Strip A is analogous to the through-width case. The constraint provided by strip B reduces $G_I$ for strip A. Conversely, strip A causes high $G_I$ at the ends of strip B when strip A pushes strip B outward. Of course, the buckled region is not comprised of strips, but this simplified interpretation helps explain the behavior observed. The following paragraphs present a more rigorous and detailed discussion of the mechanics of IRDG.

The through-width delamination will be discussed first. After describing the mechanics for the through-width delamination, its close relationship with the embedded delamination with axisymmetric loads will be discussed. Next, tractions will be applied to the through-width delamination configuration which transform it into a uniaxially loaded embedded delamination. The required tractions should give some feel for why the behaviors differ for the embedded delamination and the through-width delamination under uniaxial loads.

The discussion of the through-width delamination can be expedited by first transforming this geometrically nonlinear problem into a linear one with nonlinearly related loads (ref. 4). Fig. 8a shows a schematic of a laminate with a postbuckled through-width delamination. In fig. 8b the buckled region is replaced by the loads $P_D$ and M, the axial load and moment,respectively, in the buckled region where it is cut. The total applied load $P_T$ is equal to $P_B + P_C$. The load system in fig. 8c, (which is the same as fig. 8b) can be divided into the two load systems shown in figs. 8d and 8e. Because $P_C$ and $P_B$ are calculated using rule of mixtures, the load system in fig. 8e causes a uniform axial strain state and no interlaminar stresses. Accordingly, for strain-energy release rate calculation, the configuration in fig. 8d is equivalent to the original configuration (fig. 8a). The moment

M opens the delamination, contributing to $G_I$. It also contributes to some $G_{II}$ (ref. 4). The load ($P_C$ - $P_D$) contributes to $G_{II}$. In addition, because of the offset of the line of action of $P_C - P_D$ relative to the delamination, this force creates a moment which tends to close the delamination and reduce the $G_I$ component caused by M. The result of the competing mechanisms are strain-energy release rate variations like that in fig. 5a and 6a. The mode I strain-energy release rate first increases very rapidly with increasing strain and then decreased to zero. The mode II strain-energy release rate increases monotonically with applied load, since both M and ($P_C$- $P_D$) contribute to $G_{II}$.

The axisymmetrically loaded circular delamination is very similar to the through-width delamination. In fact, the schematics in fig. 8 are applicable if the forces are replaced by forces per unit length. The load in a column, $P_D$ is essentially constant after the applied strain is increased beyond the buckling strain, but the load in an axisymetrically loaded plate continues to increase significantly after buckling. The load $P_C$ increases linearly with the applied load. Hence, ($P_C$-$P_D$) is large for the through-width delamination but is relatively small for the axisymmetric case. As a result there is little attentuation of the effects of M by ($P_C$ - $P_D$) for the axisymmetric case. Consequently, $G_I$ is much larger for the axisymmetric case (Compare figs. 5a and 5b).

Now the uniaxially loaded embedded delamination will be considered. Figs. 9-12 illustrate the transformation of a through-width delamination (fig. 9) into an embedded delamination (fig. 12). The letters A through G are added to aid the discussion. They are not related to the letters in fig. 8. To expedite the discussion, the embedded delamination will be assumed to be rectangular. Tractions are require to close the buckled part of region AEFB. These will only be non-zero near the new delamination front and are, in fact, the interlaminar stresses.

Fig. 10 shows a slice removed from the laminate. The figure shows the forces required to close the buckled part of the boundary BF. These forces are generated when the region AEFB is closed. These forces indicate some of the interaction of regions AEFB with BFGC. There are in-plane forces $F_y$, transverse forces $F_z$, and a moment $M_y$. Fig. 11 shows the same slice after the forces have closed the buckled part of BF.

The moment $M_y$, would operate in the direction indicated in fig. 10 based on the curvature in fig. 11. Likewise, the transverse force, $F_z$, would be expected to act downward to help close the delamination front. The force, $F_y$, is a result of two things : transverse deflection and Poisson's ratio. When transverse deflection occurs, the length of a line from A to D (fig. 12) increases, hence the buckled region must be stretched in the y-direction. When the laminate is compressed in the x- direction, it expands in the y-direction due to Poisson's effect. If the base laminate has a larger Poisson's ratio than the sublaminate, then a force $F_y$ is required to enforce compatibility when the buckled part of BF is closed. The sign of $F_y$ due to Poisson's ratio would depend on the relative magnitudes of the Poisson's ratios. Differences in Poisson's ratio were not considered in this study.

The magnitude of $F_y$ is should be related to the in-plane stiffness in the y-direction. The magnitude of $M_y$ should be related to the flexural stiffness in the y-direction. The effect of material properties on $F_z$ is not as straight-forward, so no prediction will be offered.

The dimensions of the embedded delamination should affect the forces and moment. For the same transverse deflection, the curvature in the y-direction is less for a larger dimension b , so $M_y$ should decrease with increasing b. Also, the strain in the y-direction due to the increased length A-D (fig. 12) would be less for larger b. Hence, for the same transverse deflection $F_y$ should decrease with increasing b.

The moment $M_y$ should contribute primarily to $G_I$, but it also contributes to $G_{II}$. The force $F_y$ should contribute to $G_{II}$ and reduce $G_I$. The reduction is due to the offset between the delamination plane and the middle of the sublaminate. This offset causes a moment relative to the delamination plane which is opposite to $M_y$. Based on the large $G_I$ in fig. 5d, the opening effects of $M_y$ must dominate the closing effects of $F_y$.

The original configuration with a through-width delamination (fig. 9) had some distribution of $G_I$ and $G_{II}$ along x= a. The application of the forces $F_y$, $F_z$, and the moment $M_y$ changes the load flow significantly. Closing the ends of the through-width delamination (area AEFB) contributes a compressive component of interlaminar stresses along the front x=a, thus reducing $G_I$. In fact, because of this reduction, $G_I$ was zero for all strain levels at $\alpha = 90^o$ for the circular delamination under uniaxial loads. For the elliptical delamination, the magnitude of $G_I$ at $\alpha = 90^o$ was less than for the through-width delamination for the same reason (fig. 5a and 5c).

Based on the preceeding discussion, one would expect the behavior of a through-width delamination and the uniaxially loaded embedded delamination to have some similarity, but probably more differences. Fig. 5 illustrates this very well. For an embedded delamination highly elongated perpendicular to the load direction, one would expect the behavior to be like that for the through-width delamination. No highly elongated delaminations were examined in this study, but even the 1:2 aspect ratio ellipse has a $G_I$ variation at $\alpha = 90^o$ (fig. 5c) which is very similar to that for a through-width delamination (fig. 5a) . But this similarity has little importance for this case, since the $G_I$ was very much larger at $\alpha = 0^o$ (fig. 5d).

## SUMMARY

The variation of strain-energy release rate with applied strain was shown to be dramatically different for the through-width delamination and the embedded delamination. Both axisymmetric and uniaxial loads were considered for the embedded delamination. These divergent behaviours were explained in terms of the mechanisms which create the strain-energy release rates.

Earlier studies described the mechanics of instability-related delamination growth

(IRDG) for the through-width delamination. For completeness these earlier results were discussed herein. This paper also describes the mechanics of IRDG for the embedded delamination. The mechanics for the axisymmetric case were found to be very similar to that for the through-width delamination. Large differences in $G_I$ observed for the through-width and axisymmetric cases could be explained by the different mix of secondary forces that generate strain-energy release rate. The uniaxially loaded embedded delamination has a much more complicated response than either the through-width or axisymmetric cases. By starting with a through-width delamination and applying tractions, one can transform it into an embedded delamination. Examination of these tractions explains why the uniaxially loaded embedded delamination behaves very differently than either the through-width or the axisymmetric cases.

## REFERENCES


1. Konishi, D. Y. and Johnson, W. R.: Fatigue Effects on Delaminations and Strength Degradation in Graphite/Epoxy Laminates. Composite Materials: Testing and Design, Fifth Conference, ASTM STP 674, American Society for Testing and Materials, 1979, pp. 597-619.

2. Whitcomb, John D.: Finite Element Analysis of Instability Related Delamination Growth. J. Composite Materials, Vol. 15, Sept. 1981., pp. 403-426

3. Shivakumar, K. N. and Whitcomb, J. D.: Buckling of a Sublaminate in a Quasi-Isotropic Composite Laminate. Journal of Composite Materials, Vol. 19, Jan. 1985.

4. Whitcomb, John D.: Parametric Analytical Study of Instability - related Delamination Growth. Composites Science and Technology, 25, 1986, pp.19-48

5. Chai, Herzl; Babcock, Charles D. and Knauss, Wolfgang G.: One Dimensional Modelling of Failure in Laminated Plates by Delamination Buckling. Int. J. Solids Structures, Vol. 17, No. 11, 1981, pp. 1069-1083.

6. Chai, Herzl and Babcock, Charles D.: Two-Dimensional Modelling of Compressive Failure in Delaminated Laminates. J. Composite Materials, Vol. 19, Jan. 1985, pp. 67-98.

7. Whitcomb, John D. and Shivakumar, K. N.: Strain-Energy Release Rate Analysis of a Laminate With a Postbuckled Delamination. Fourth International Conference on Numerical Methods in Fracture Mechanics Pineridge Press, 1987, pp. 581-605. Also available as NASA TM 89091.

8. Whitcomb, John D. : Three-Dimensional Analysis of a Postbuckled Embedded Delamination. NASA TP 2823, 1988.

9. Bottega, William J. : The Mechanics of Delamination in Composite Materials. PhD thesis, Yale University, May, 1984.

10. Frederick, D. and Chang, T. S.: Continuum Mechanics. Scientific Publishers, Inc., Cambridge, 1972, pp. 79-82.

11. Zienkiewicz, O. C.: Incremental Displacement in Non-linear Analysis, in International Journal for Numerical Methods in Engineering, vol. 3, 1971, pp. 587-592.

12. S. S. Wang and Choi, I.: The Mechanics of Delamination in Fibre- reinforced Composite Laminates. Part I- Stress Singularities and Solution Structure. Part II- Delamination Behavior and Fracture Mechanics Parameters. NASA CR 172269 and 172270, Nov. 1983.

13. Rybicki, E. F. and Kanninen, M. F.: A Finite Element Calculation of Stress Intensity Factors by a Modified Crack Closure Integral. Engineering Fracture Mechanics, 1977, Vol. 9, pp. 931-938.

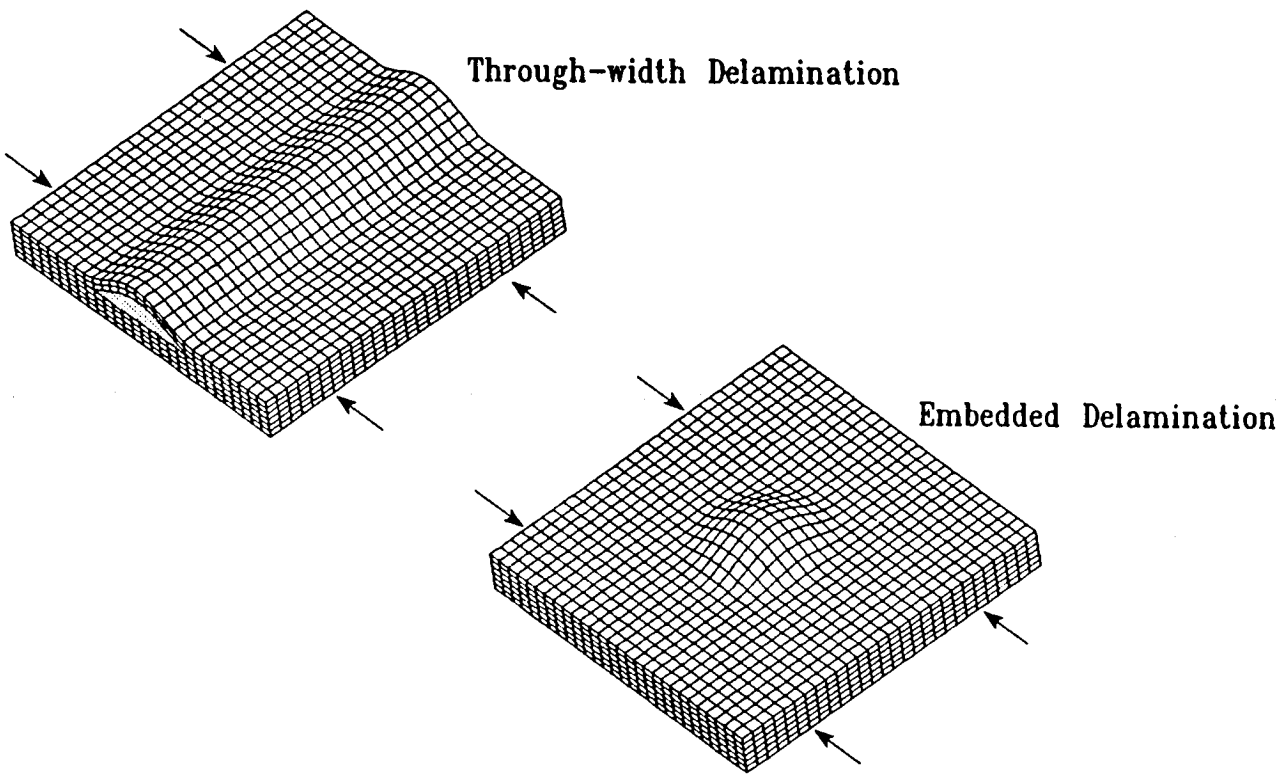


Fig. 1 Two configurations which exhibit instability-related delamination growth.

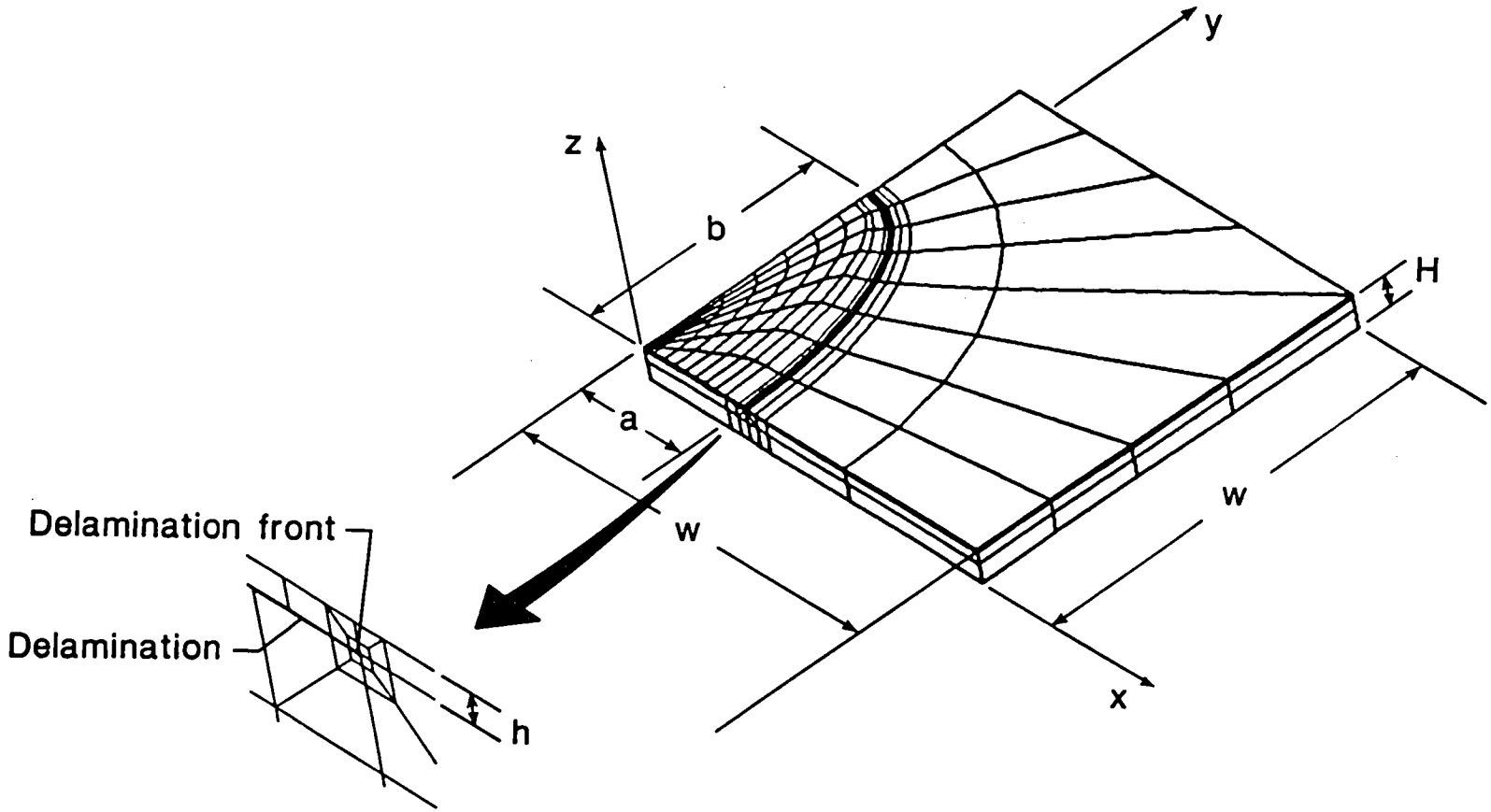


(a) Embedded delamination

Fig. 2 Typical finite element models.

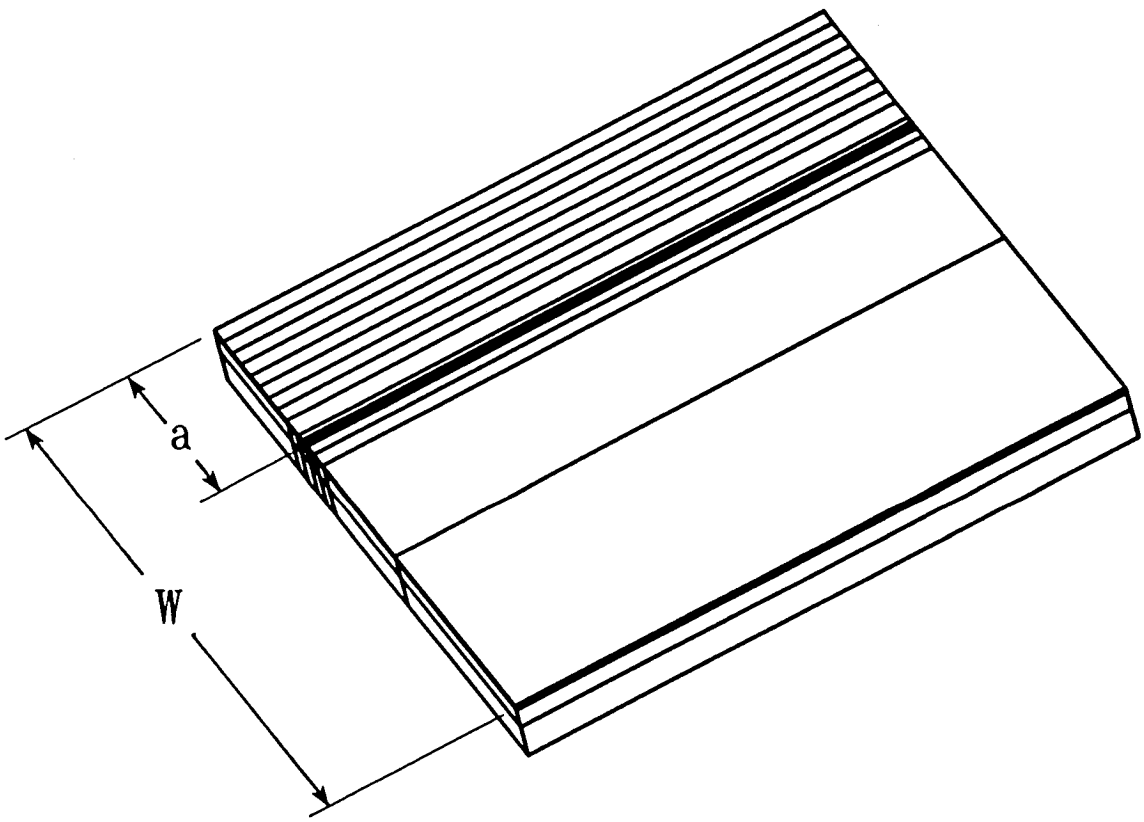


(b) Through-width delamination

Fig. 2, concluded.

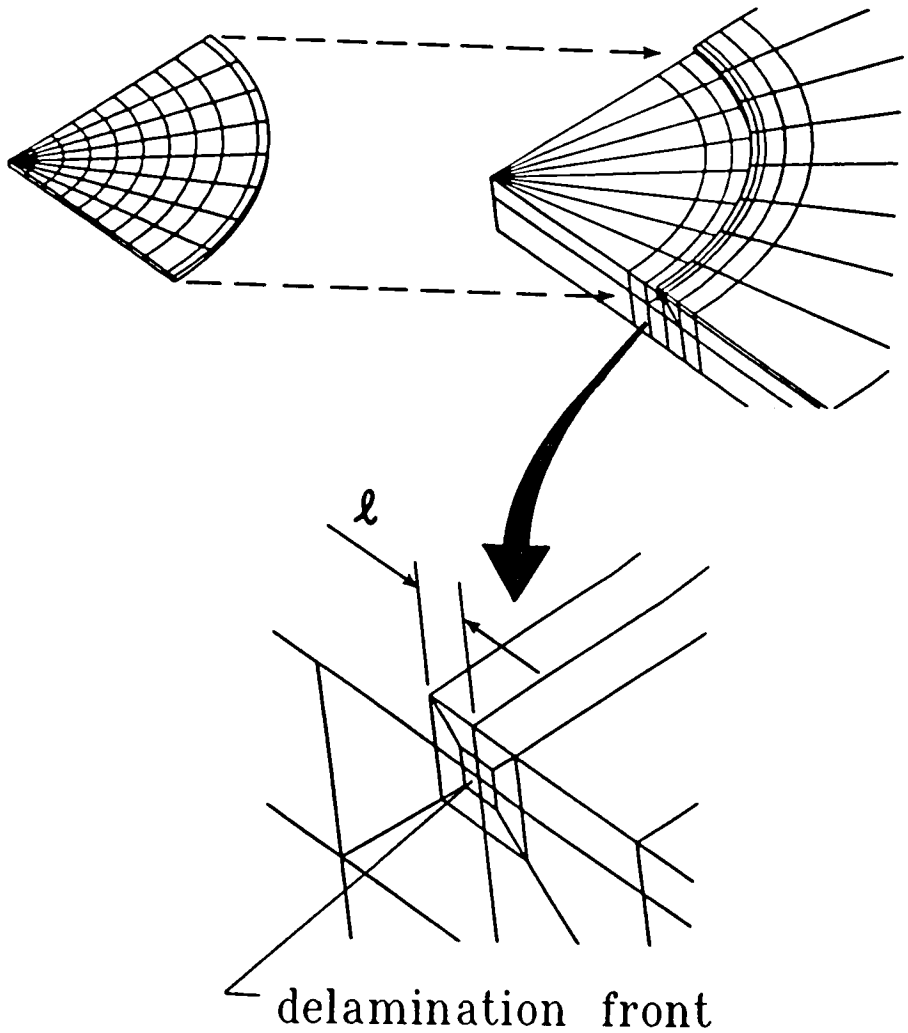


Fig. 3 Typical model after division into substructures.

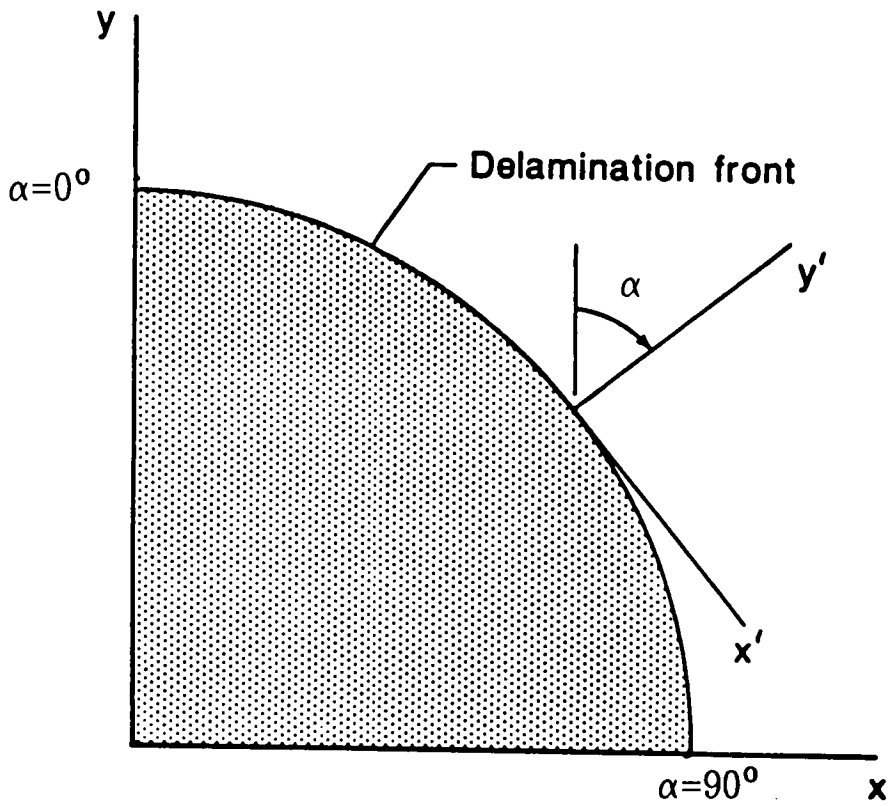


Fig. 4 Global and local coordinate systems.

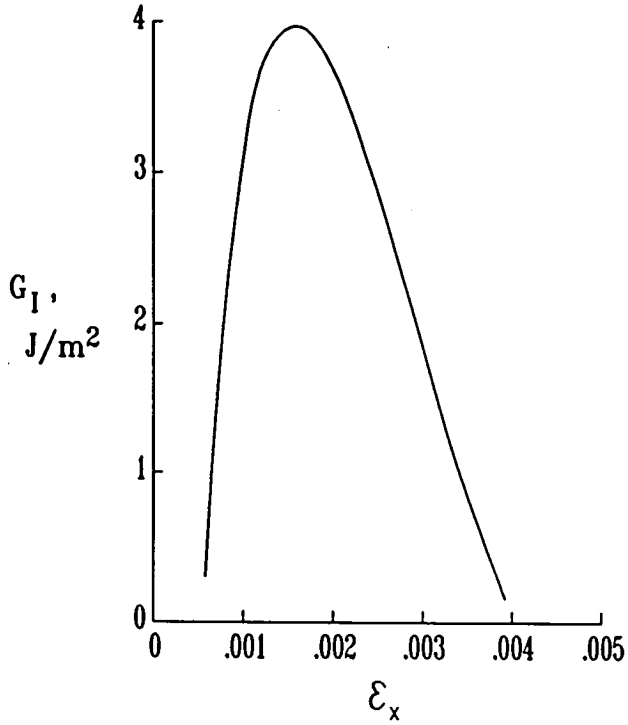


(a) Through-width delamination

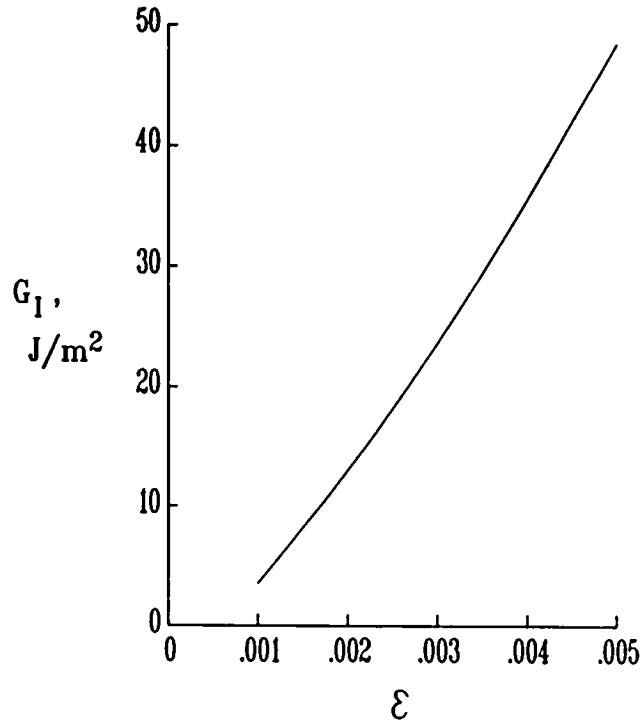


(b) Embedded delamination with axisymmetric load

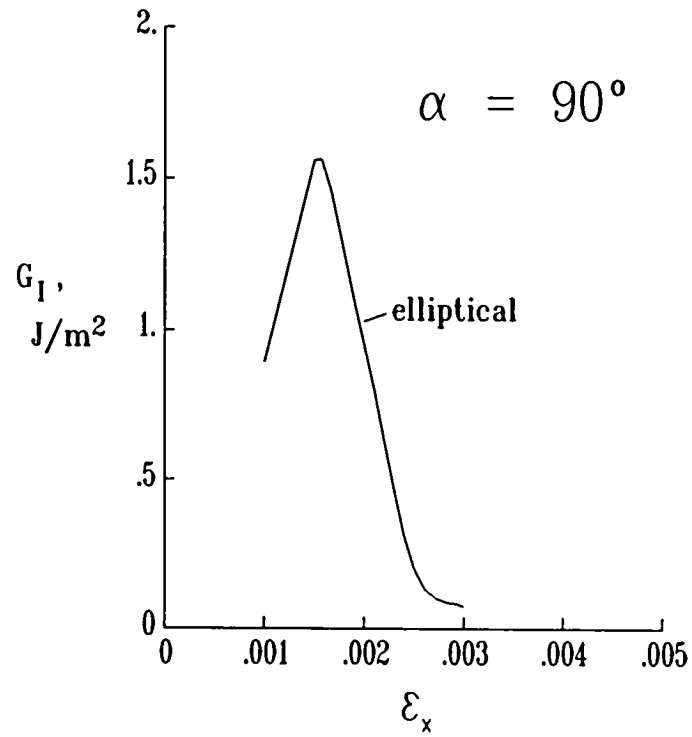


(c) Embedded delamination with uniaxial load

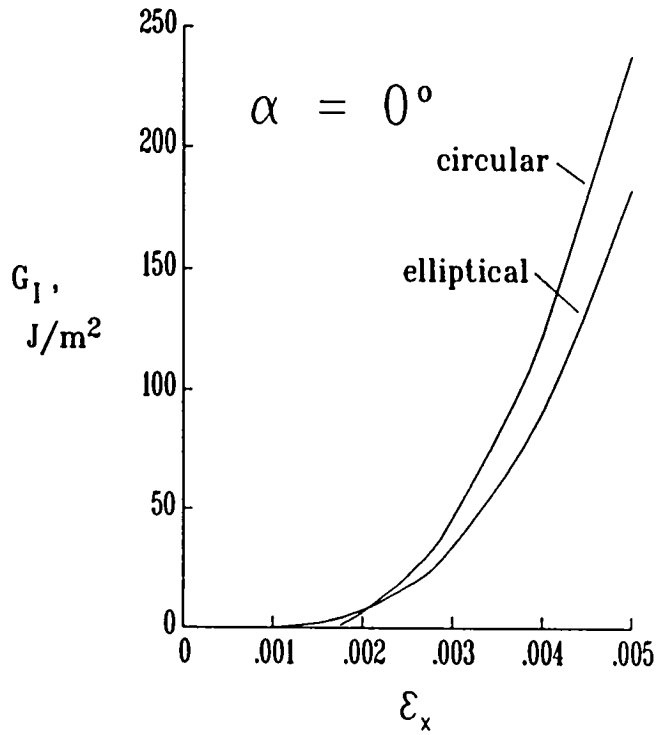


(d) Embedded delamination with uniaxial load

Fig. 5 Effect of strain level on strain-energy release rate

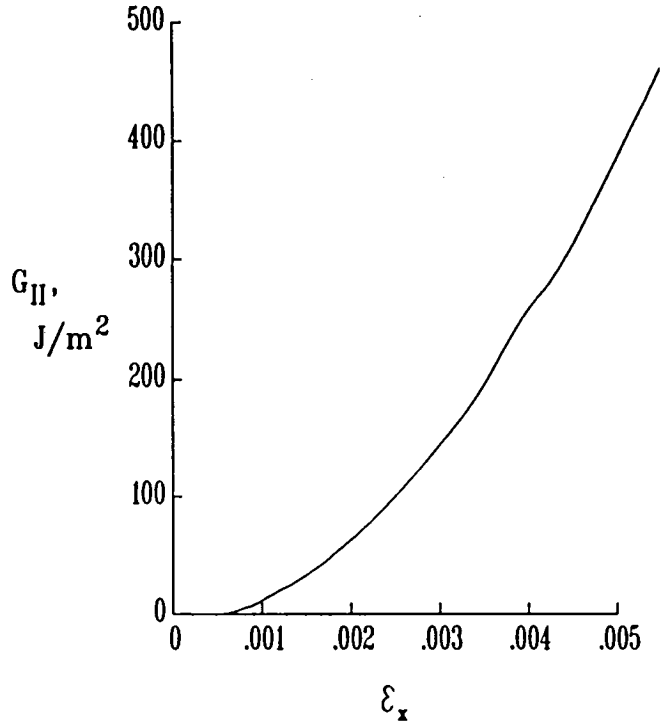


(a) Through-width delamination

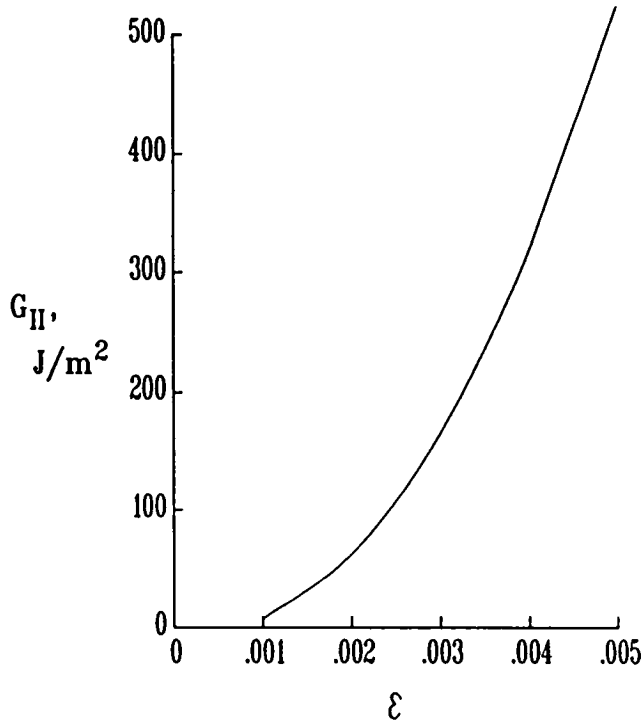


(b) Embedded delamination with axisymmetric load

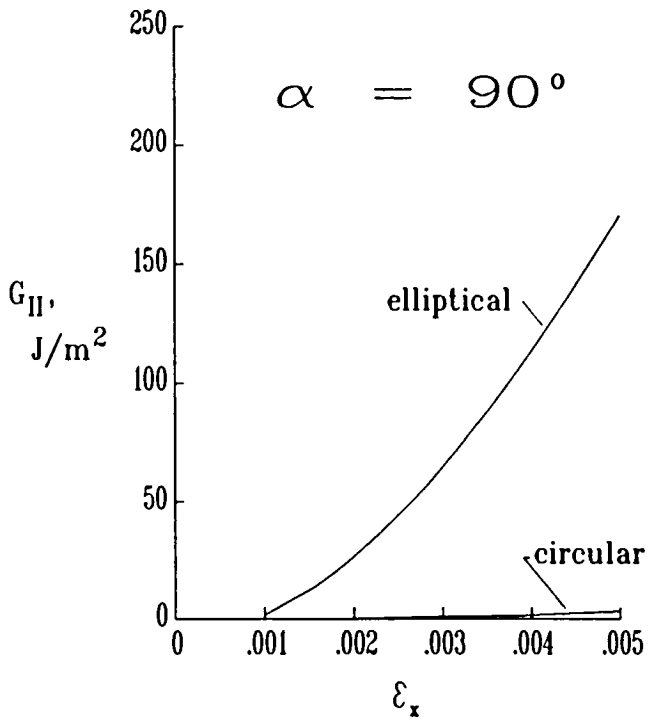


(c) Embedded delamination with uniaxial load

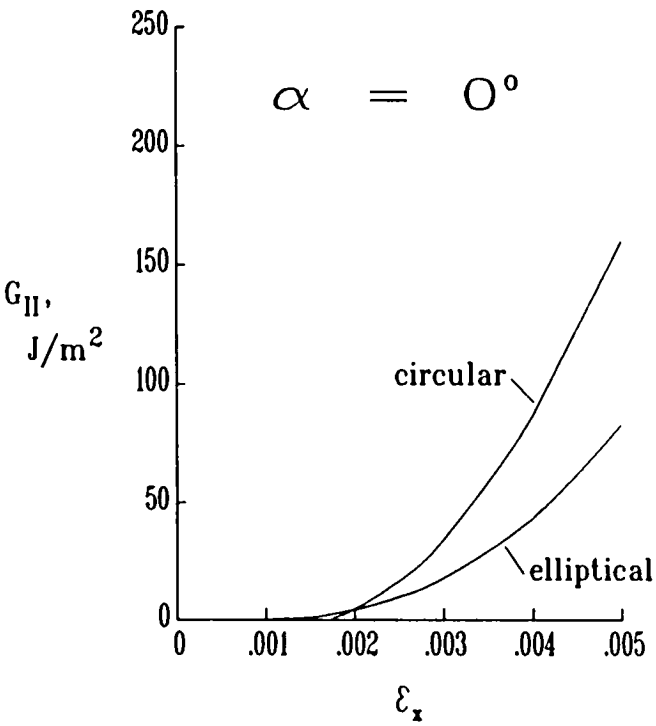


(d) Embedded delamination with uniaxial load

**Fig. 6 Effect of strain level on mode II strain-energy release rate**

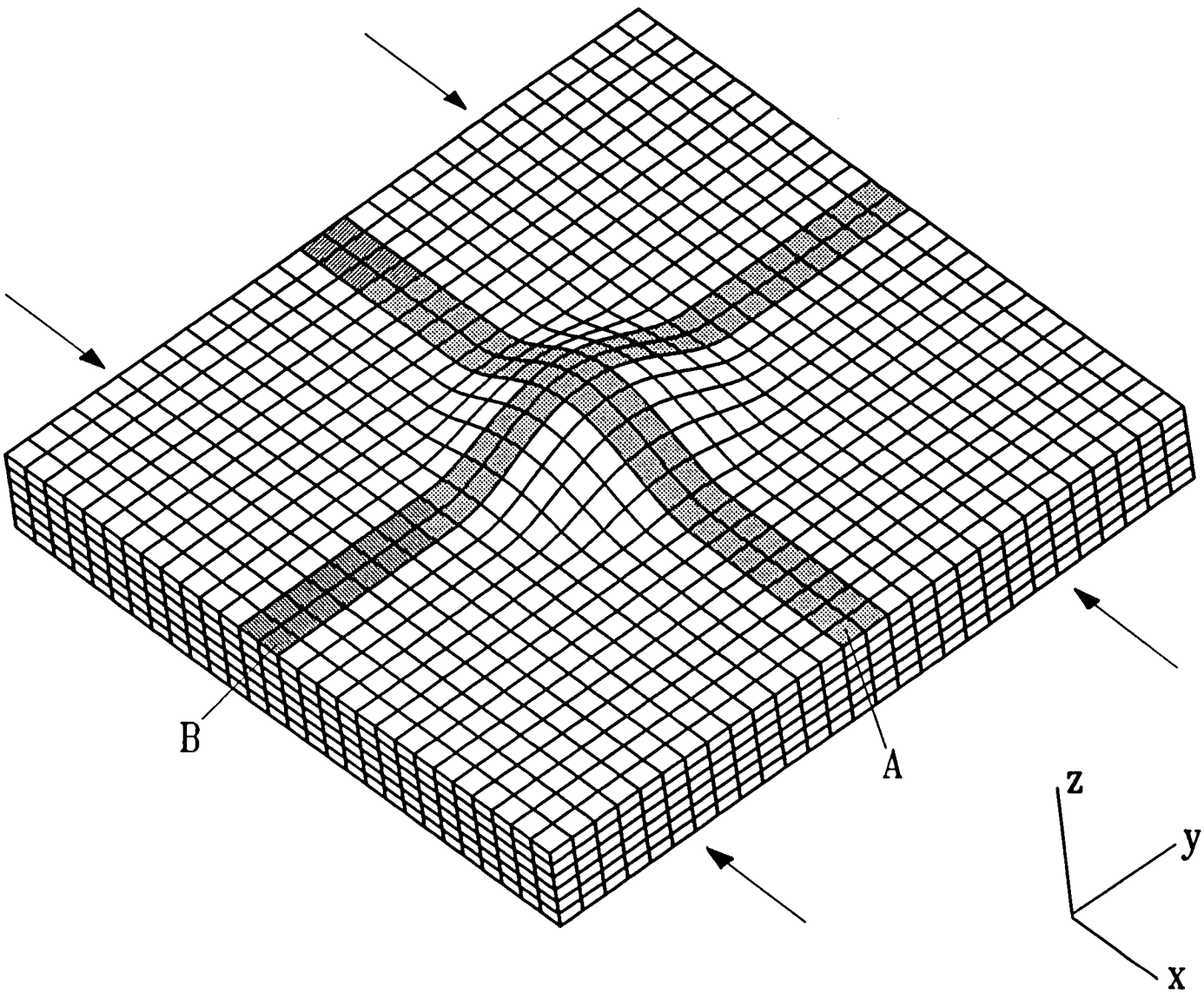


Fig. 7 Strips of sublaminate aligned perpendicular and parallel to the load direction.

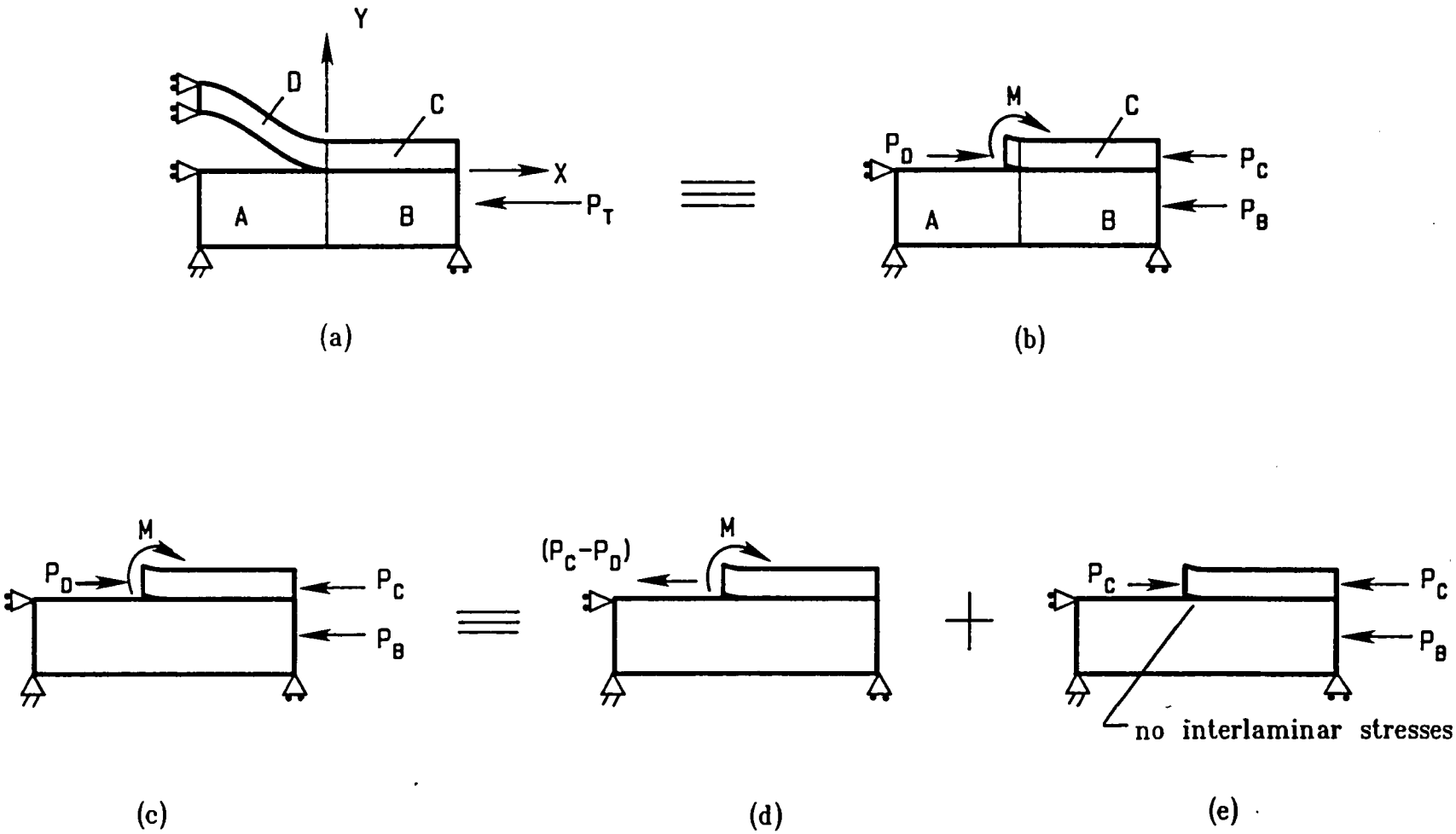


Fig. 8 Nonlinear configuration (a) transformed into linear configuration (d) with two nonlinearly related loads ($P_C - P_D$) and M.

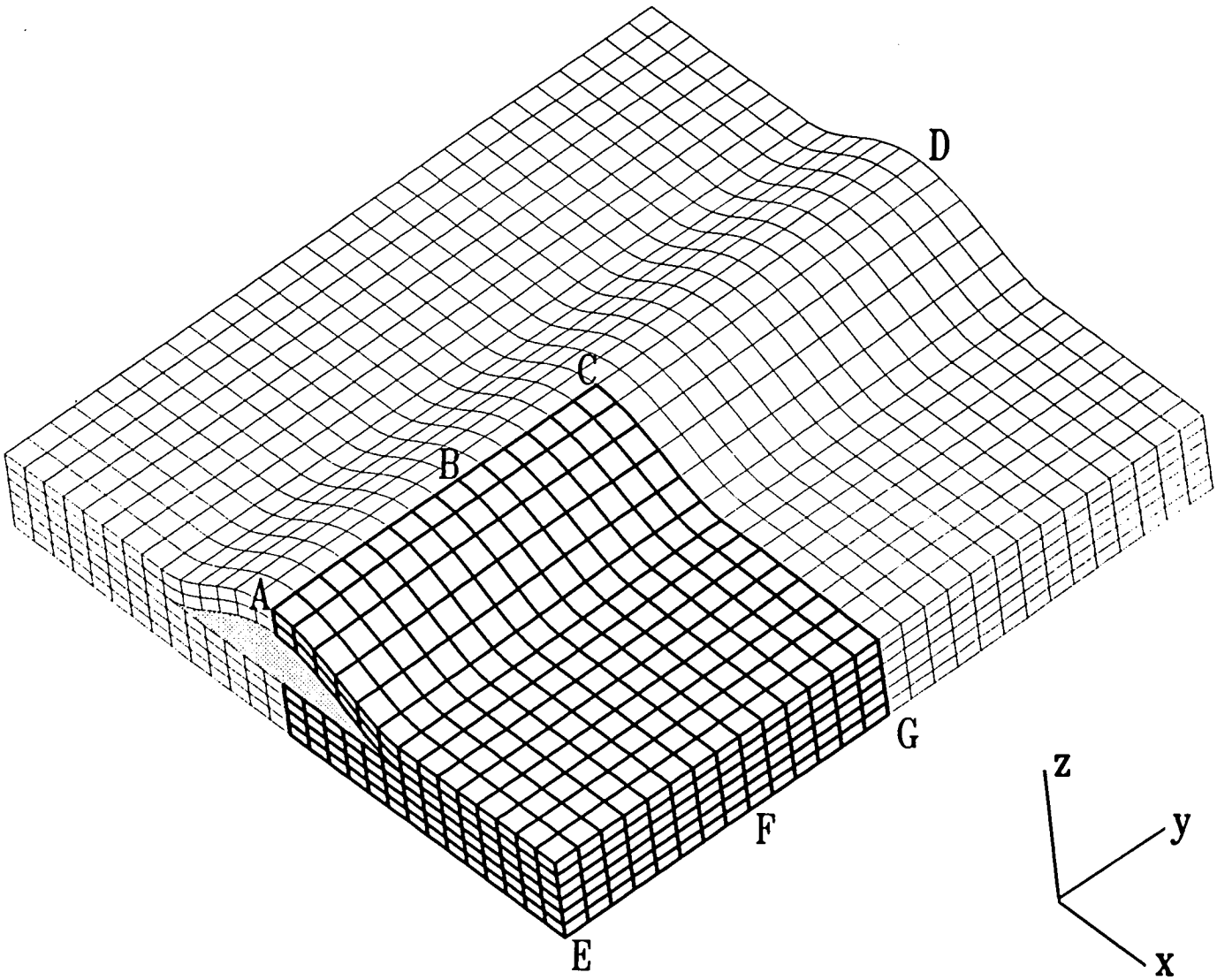


Fig. 9 Schematic for transformation of through-width delamination into an embedded delamination.

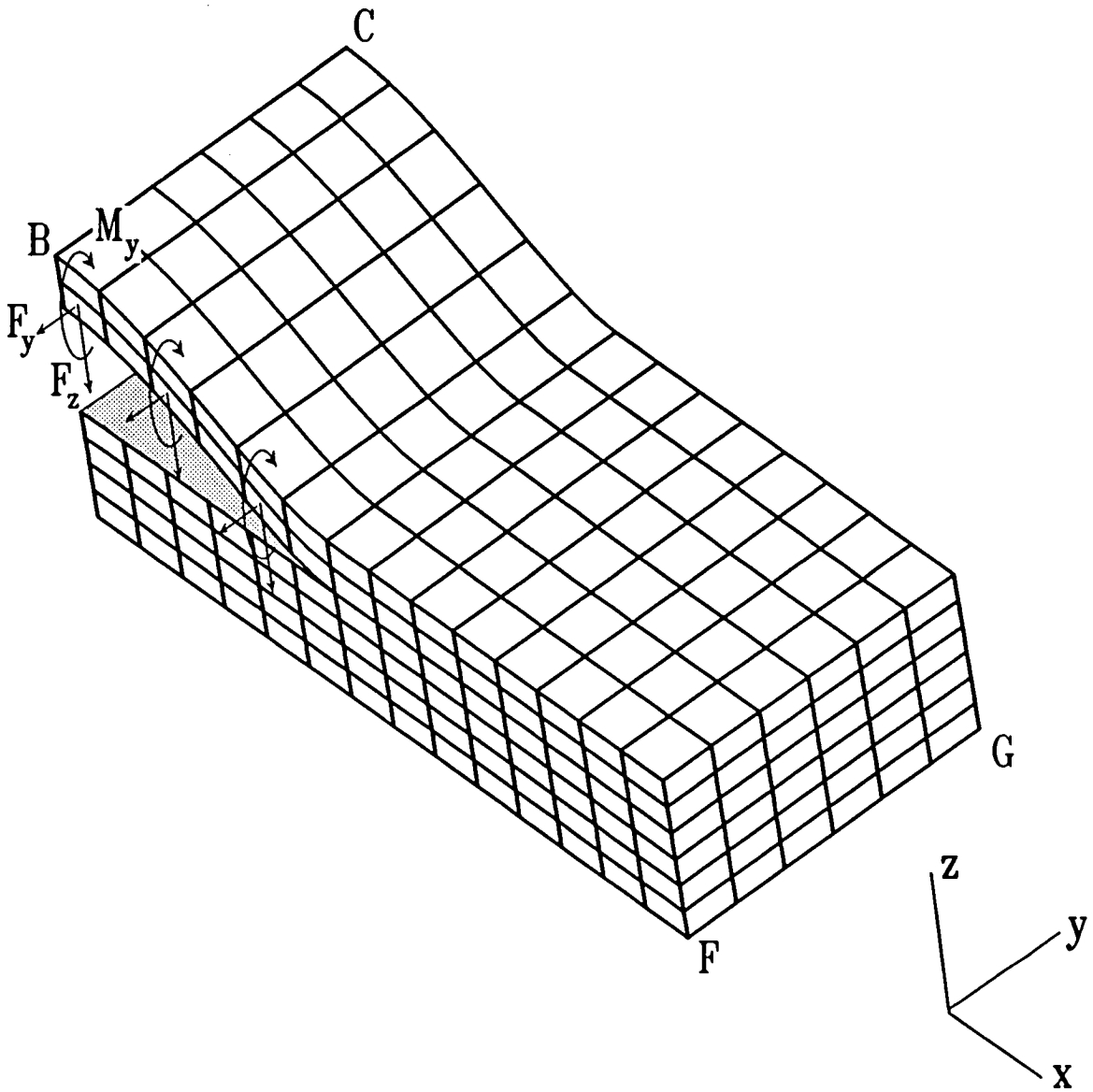


Fig. 10 Slice of laminate showing tractions required to perform transformation by closing buckled part of boundary BF

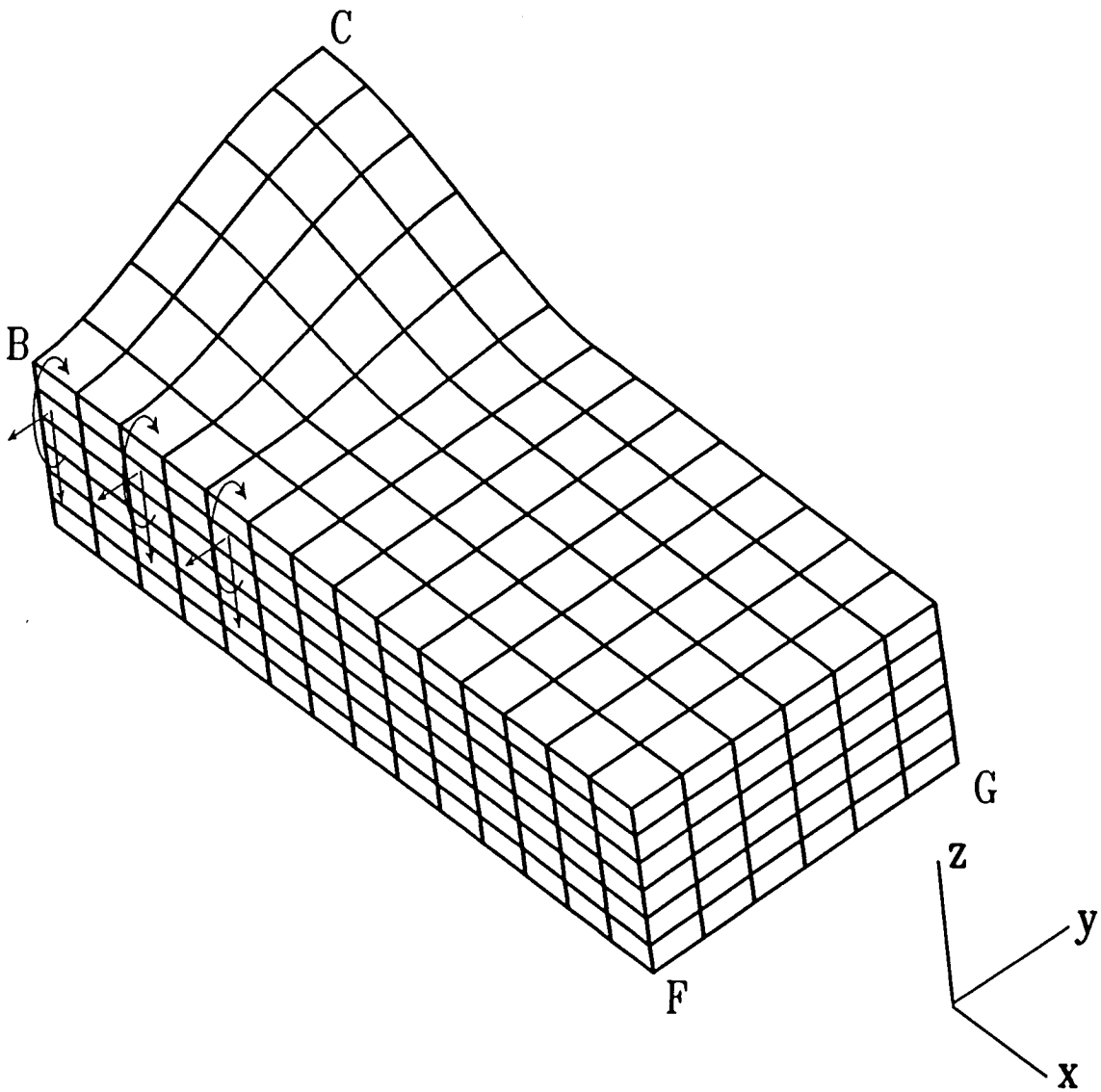


Fig. 11 Slice of laminate after tractions have closed boundary

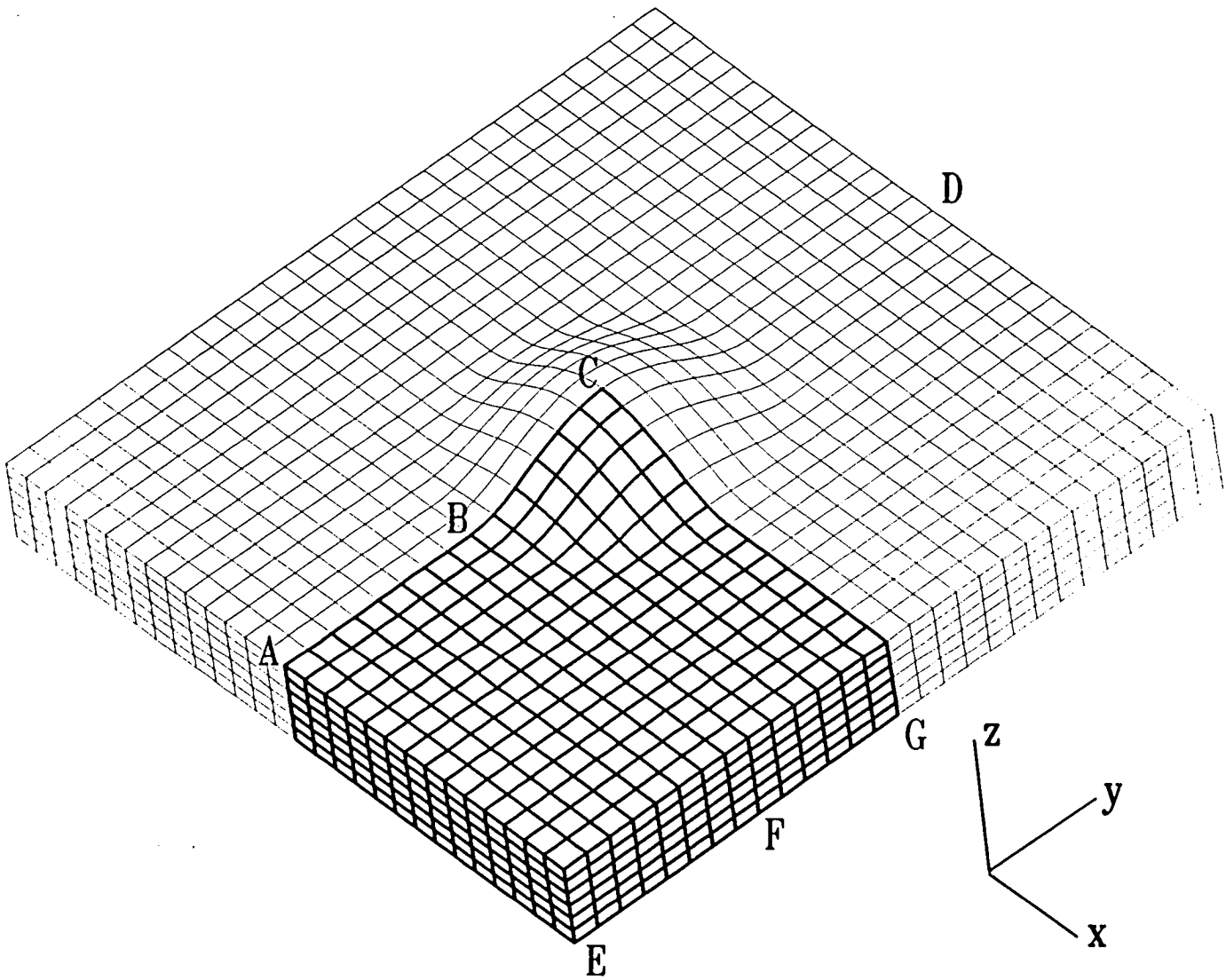


Fig. 12 Entire laminate after transformation to embedded delamination

Standard Bibliographic Page

| 1. Report No. | 2. Government Accession No. | 3. Recipient's Catalog No. |
|---|---|---|
| NASA TM-100622 | | |

| 4. Title and Subtitle | 5. Report Date |
|---|---|
| MECHANICS OF INSTABILITY-RELATED DELAMINATION GROWTH | May 1988 |
| | 6. Performing Organization Code |
| 7. Author(s) | 8. Performing Organization Report No. |
| John D. Whitcomb | |
| 9. Performing Organization Name and Address<br>National Aeronautics and Space Administration<br>Langley Research Center<br>Hampton, Virginia 23665-5225 | 10. Work Unit No.<br>505-63-01-05 |
| | 11. Contract or Grant No. |
| 12. Sponsoring Agency Name and Address<br>National Aeronautics and Space Administration<br>Washington, DC 20546-0001 | 13. Type of Report and Period Covered<br>Technical Memorandum |
| | 14. Sponsoring Agency Code |

15. Supplementary Notes

16. Abstract

Local buckling of a delaminated group of plies can lead to high interlaminar stresses and delamination growth. The mechanics of instability-related delamination growth (IRDG) had been described previously for the through-width delamination. This paper describes the mechanics of IRDG for the embedded delamination subjected to either uniaxial or axisymmetric loads. The mechanics of IRDG are used to explain the dramatic differences in strain-energy release rates observed for the through-width, the axisymmetrically loaded embedded delamination, and the uniaxially loaded embedded delamination.

| 17. Key Words (Suggested by Authors(s)) | 18. Distribution Statement |
|---|---|
| Buckling<br>Local buckling<br>Compression<br>Delamination<br>Strain-energy release rates | Unclassified - Unlimited<br>Subject Category - 39 |

| 19. Security Classif.(of this report) | 20. Security Classif.(of this page) | 21. No. of Pages | 22. Price |
|---|---|---|---|
| Unclassified | Unclassified | 25 | A02 |

For sale by the National Technical Information Service, Springfield, Virginia 22161